## Quasi-amorphous crystal

O.U. Salman, 1,2 A. Ahadi, 2 and L. Truskinovsky 3

<sup>1</sup>LSPM, CNRS UPR3407, Université Sorbonne Paris Nord, 93400, Villateneuse, France <sup>2</sup>Lund University, Department of Mechanical Engineering Sciences, SE-221 00 Lund, Sweden <sup>3</sup>PMMH, CNRS UMR 7636 ESPCI PSL, 10 Rue Vauquelin, 75005, Paris, France (Dated: November 12, 2025)

Brittle plastic yielding is a salient feature of well-annealed glassy materials. Here we show that the same behavior is characteristic of perfect crystals after they experience mechanically driven elastic instability leading to massive nucleation of dislocations. We argue that such 'preparation' effectively converts an atomic configuration from crystalline to quasi-amorphous. To understand the nature of the subsequent mechanical response, which is reminiscent of quasi-brittle yielding we study an athermal model 2D crystal subjected to quasistatic loading. We show that the intermittent pre- and post-yield dislocation avalanches exhibit power law statistics with matching exponents. The computed value of these exponents is indicative of marginal stability.

The complexity of plastic behavior of crystalline solids is revealed by pre- and post-yield intermittent fluctuations accompanied by scale-free organization of dislocations [1–10]. Such features are also typical of amorphous plasticity [11–20]. To build a conceptual link between the two phenomena, we study in this Letter a relatively transparent prototypical example of a 2D square crystal subjected to quasistatic loading in athermal conditions.

To prepare a 'generic' crystal we start with a pristine dislocation-free configuration and bring the associated perfect crystal to the point of mechanical instability which is resolved through massive dislocation nucleation. We argue that such 'preparation' effectively converts an atomic configuration from crystalline to quasi-amorphous [21–23]. The subsequent plastic flow begins with a hardening stage, which involves a superposition of spatially localized dislocation rearrangements. This 'microplasticity' regime is terminated abruptly with a quasi-brittle yield leading to the formation of multi-grain pattern involving global shear bands. The postyield plastic flow is characterized by a stress plateau with superimposed fluctuations representing broadly distributed dislocation avalanches. Similar quasi-brittle yield has been observed in well-annealed glasses [24–32]. Despite the absence of dislocations in amorphous plasticity, behind both phenomena is an evolving elastic incompatibility [33–37] with underlying elementary mechanical events represented by shear eigenstrains [38–40].

To reveal the universal features of the criticality exhibited by crystal and amorphous plasticity, we perform a detailed study of dislocation dynamics in a prototypical athermal square crystal subjected to quasistatic loading by shear strain applied along one of the slip directions. Our main tool is a novel mesoscopic tensorial model (MTM) of crystal plasticity representing a conceptual trade-off between continuum and atomic descriptions [41–48]. Crucially, it allows one to capture the intermittent nature of dislocation avalanches while resolving topological transitions involved in nucleation and annihilation of dislocations without any specialized phenomenological assumptions [49]. In contrast to other computational approaches to micro-scale plasticity [50–75] the MTM allows one to deal with statistically meaningful number of dislocations while accounting adequately for large lattice rota-

tions and presenting geometrically exact description of lattice-invariant shears [76–79].

The main idea of the MTM approach is to associate with material points an effective energy landscape whose tensorial periodicity accounts for crystallographically-invariant deformations. The resulting Landau-type model is characterized by infinitely many equivalent energy wells [41-48, 80-90] and plastically deformed crystals emerge as a multi-phase mixtures with dislocations playing the role of effective domain boundaries. The small scale regularization is achieved by mesoscopic discretization. Despite operating with engineering concepts of stress and strain the resulting computational code correctly captures not only long-range elastic interactions of dislocations but also describes adequately their short-range interactions involved in the formation of complex dislocational entanglements. Some elements of the MTM approach can be found in [91–97], see also some parallel recent developments in [98–100].

Consider the continuum deformation field  $\mathbf{y} = \mathbf{y}(\mathbf{x})$ , where  $\mathbf{y}$  and  $\mathbf{x}$  are positions of material points in the current and reference configurations, respectively. Due to frame indifference constraint, the strain energy density  $\varphi$  can depend on the deformation gradient  $\mathbf{F} = \nabla \mathbf{y}$ , only through the metric tensor  $\mathbf{C} = \mathbf{F}^T \mathbf{F}$  which then plays the role of a tensorial order parameter. The function  $\varphi(\mathbf{C})$  should respect the symmetry of an underlying Bravais lattice extended beyond the conventional point group. For instance, to capture lattice invariant shears in 2D theory we should require that

$$\varphi(\mathbf{C}) = \varphi(\mathbf{m}^T \mathbf{C} \mathbf{m}),\tag{1}$$

with the unimodular integer valued matrix  $\mathbf{m}$  belonging to  $GL(2,\mathbb{Z})$ , see [101] for details. In view of this symmetry, the surface  $\det \mathbf{C}=1$  in the 3D space  $(C_{11},C_{22},C_{12})$  is tessellated into an infinite number of equivalent periodicity domains; if the energy density is known in one of such domains, it can be extended to the whole configurational space by  $GL(2,\mathbb{Z})$  symmetry. To visualize this tessellation, it is convenient to project stereographically the infinite surface  $\det \mathbf{C}=1$  on a unit (Poincaré) disk, see Fig. 1 where we show in gray the fundamental (minimal periodicity) domain  $\mathscr{D}$ .

In our numerical experiments we used the polynomial function  $\varphi(\mathbf{C})$  proposed in [89] which is the simplest to ensure

stress continuity, see [101] for details. In Fig. 2 we illustrate the corresponding multi-well energy landscape with equivalent energy wells representing replicas of the reference square lattice. One can see that such a landscape contains a network of low energy valleys depicting in our case simple shears parallel to crystallographic slip planes and therefore mimicking the conventional plastic 'mechanisms' operating in square crystals.

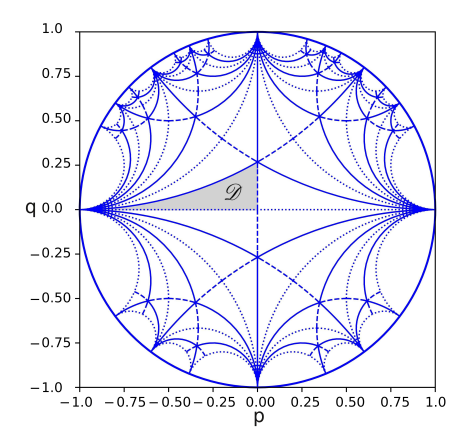


FIG. 1.  $GL(2,\mathbb{Z})$ -induced tessellation of the configuration space of metric tensors  $C_{11},C_{22},C_{12}$  with  $\det \mathbf{C}=1$  stereographically projected on the Poincaré disk  $p^2+q^2<1$  where  $p=t(C_{11}-C_{22})/2, q=tC_{12}$ , and  $t=2/(2+C_{11}+C_{22})$ . The highlighted domain  $\mathscr D$  is the fundamental (minimal periodicity) domain.

The presence of the energy barriers separating individual energy wells makes the function  $\varphi(\mathbf{C})$  highly nonconvex, see Fig. 2. Therefore, the corresponding scale-free Landau model is degenerate and needs to be regularized through the introduction of a cut-off length scale. This is achieved in the MTM by projecting the continuum problem on a uniform mesoscale grid and associating the periodic elastic energy with discrete elements whose linear size h becomes a physical parameter. In this way the infinite dimensional space of continuum deformation fields is reduced to a finite dimensional set of compatible, piece-wise affine mappings, see [101] for details.

The driven system of this type will experience a rich repertoire of instabilities. Specificaly, an incremental elastic energy minimization of a system subjected to quasistatic loading will generically lead to repeated jump discontinuities representing branch switching events. The energy losses associated with such jumps will represent plastic dissipation; in the continuum limit the jumps will merge giving rise to rate-independent plasticity [102].

In our numerical experiments a square crystal was represented by  $N \times N$  nodes, with N=400. The nodes were arranged into triangular finite elements. We loaded the corresponding athermal system quasi-statically by applying the affine displacement field

$$\mathbf{u}(\alpha, \mathbf{x}) = (\bar{\mathbf{F}}(\alpha) - 1)\mathbf{x},\tag{2}$$

with

$$\bar{\mathbf{F}}(\alpha) = \mathbf{I} + \alpha \mathbf{e}_1 \otimes \mathbf{e}_2$$

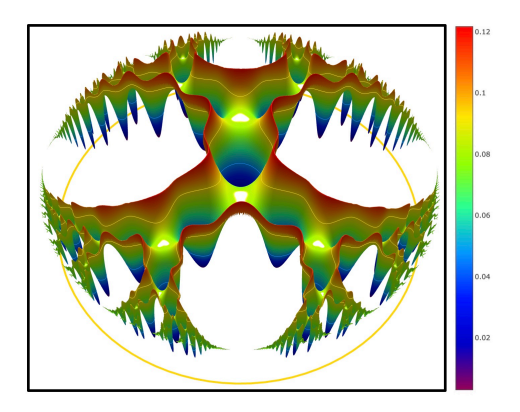


FIG. 2. Energy landscape in the space of metric tensors (Poincaré) disk shown in Fig. 1. Color indicates the energy level with only the lowest energy levels shown. The deepest energy wells correspond to equivalent representations of the same square lattice.

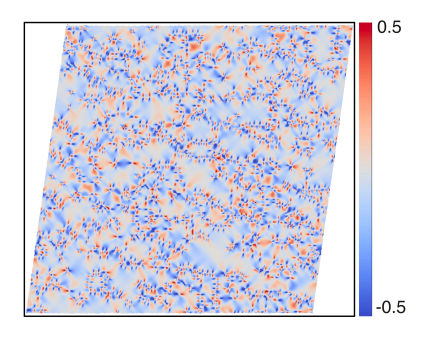


FIG. 3. Dislocated configuration emerging after a homogeneous lattice is mechanically driven to the threshold of elastic instability. Colors indicate the level of the shear component of the Cauchy stress tensor  $\sigma_{xy}$ . The highest stress levels of both signs correspond to the location of dislocation cores.

where  $\mathbf{e}_i$ , i=1,2, is the orthonormal basis of the reference square lattice. In this way we imposed simple shear along one of the principal slip directions with shear amplitude  $\alpha$  serving as the loading parameter. By changing this parameter in strain increments of order  $10^{-6}$ , we advanced the loading. After each such increment the displacement field was updated by the energy minimization algorithm. Details of the discretization, of the incremental energy minimization algorithm and of the implementation of the loading protocol under periodic boundary conditions can be found in [101].

To obtain a 'generic' sample, we first loaded a pristine (defect-free) crystal till the affine configuration became elastically unstable. The corresponding critical value of the loading parameter  $\alpha=\alpha_c\approx 0.138$  is very close to the threshold of positive definiteness of the acoustic tensor [103–105], see the explicit formulas in [101]. The breakdown of an elastic state takes the form of a major system-size inelastic event. It leads to multiple nucleation of dislocations which apparently transforms a perfect crystal into a quasi-amorphous system, see Fig. 3. We observe that the unfolding of the elastic instability is arrested at a state which one can expect to be only

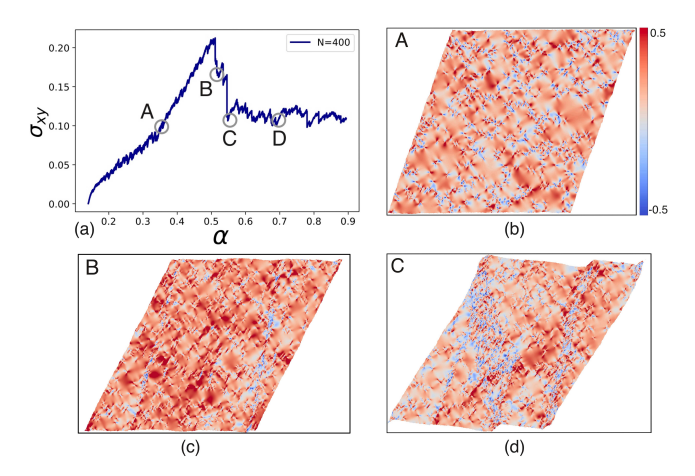


FIG. 4. (a) Stress-strain response of a quasi-amorphous crystal shown in Fig. 3. (b) Dislocated configuration in a typical preyield state characterizing the stage of 'microplasticity'. (c,d) Dislocated configuration characterizing different stages of unfolding of the quasi-brittle system size event. Colors indicate the level of the shear component of the Cauchy stress tensor  $\sigma_{xy}$ .

marginally stable.

We continued to load the obtained 'generic' sample using the same athermal quasistatic protocol and the ensuing stress-strain response is shown in Fig. 4(a). Its salient feature is the presence of irregularly placed elastic branches interrupted by intermittent stress drops; the latter represent plastic avalanches involving partial unlocking of dislocation structures. Among these avalanche-type events, one major stress drop stands out and can be interpreted as a plastic yield separating two different regimes. While the first (pre-yield) regime is characterized by quasi-elastic hardening, the second (post-yield) regime is represented by a stress plateau which suggests quasi-stationary plastic flow, see Fig. 4(a).

Our Fig. 4(b) illustrates the stress field in a typical pre-yield state A. The restructuring of the dislocation pattern is relatively minor with dislocations moving only between the pre-existing locking sites, cf. Fig. 3. Such response is known to be a characteristic pre-yield feature for both amorphous and (defective) crystalline solids [4, 106–110]. This 'microplasticity' regime ends with the system-size event reminiscent of quasi-brittle plastic yield encountered in well-annealed glasses and also in some sub-micron crystals [111–121]. As we see from Fig. 4(a) it takes the form of a two-stage transition  $A \rightarrow B \rightarrow C$ ; the snapshots of the spatial stress configurations in the states B and C are shown in Fig. 4(c,d). The associated global restructuring reveals collective dislocation activity manifested through the emergence of system-spanning shear bands.

Additional details can be seen in Fig. 5 where we illustrate the strain-energy density field in the state C. We see the development of low-energy rotated patches of the original lattice forming intricate polycrystalline grain texture with misorientation of neighboring grains controlled by the overall compatibility of the deformation field as explained in [47]; the elastic energy is localized around dislocation-rich grain

boundaries. In the inset in Fig. 5 we made dislocations of different sign clearly visible: they were identified via Delaunay triangulation and nodes with five/seven neighbors are shown in blue/red. One can see the emergence of energy minimizing structure of grain boundaries [122–124] with ubiquitous presence of  $\Sigma$ 5 grain boundaries, see [47] for the explanation.

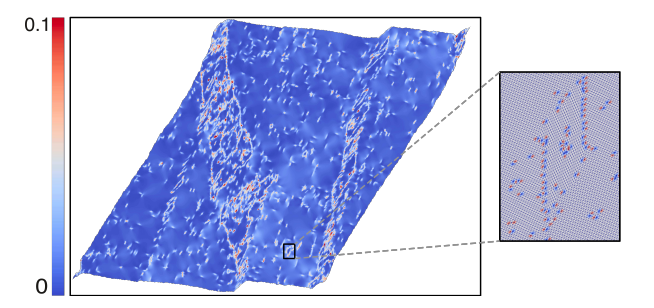


FIG. 5. The micro-configuration configuration corresponding to the state C marked in Fig. 4. Colors indicate the magnitude of strainenergy density. The inset shows a single grain and details the dislocation structure of the grain boundaries.

The post-yield regime, characterized by relative stabilization of the average stress level, can be interpreted as a quasistationary non-equilibrium steady state (NESS). A representative snapshot of the micro-configuration of the crystal in the state D is shown in Fig. 6 where we see further development of the polycrystalline grain texture. During intermittent avalanches characterizing this regime larger grains occasionally merge while small grains continue to emerge. In this way the self-organization of dislocations continues to generate additional scales which contribute to the formation of the global hierarchical structure. Through the transitions from isolated dislocation motion to collective dislocation behavior the system acquires access to a much broader repertoire of relaxation mechanisms. A detailed analysis of the avalanche structure shows that while in the pre-yield regime plastification takes place primarily in the form of isolated, linear arrangements of transformed elements, a typical post-yield avalanche reveals extended plastified regions with complex branching.

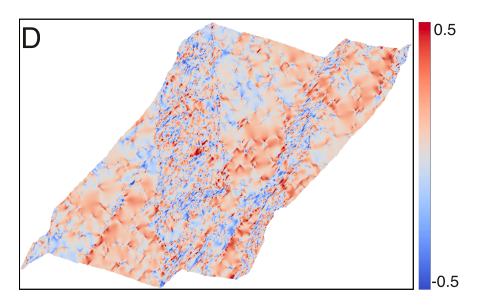


FIG. 6. Mature shear bands in the regime of stationary post-yield plastic flow represented by the state D marked in Fig. 4. Colors indicate the level of the shear component of the Cauchy stress tensor  $\sigma_{xy}$ .

An important window into the micro-mechanics of solids

undergoing plastic flow is provided by the study of the statistical structure of plastic fluctuations [1, 4, 22, 125–128]. Thus, it is known that in amorphous solids the probability distribution of the energy drops associated with individual avalanches  $\Delta W = W_{\rm before} - W_{\rm after},$  where W is the total elastic energy of the crystal defined in [101], is represented by power laws of the form

$$P(x) \sim x^{-\epsilon} e^{-\lambda x} \tag{3}$$

with the same exponent  $\epsilon$  but different values of the cut-off parameter  $\lambda$  for pre-yield and post-yield regimes [39, 129–131]. Our results, illustrated in Fig. 7, show that for 'generic' crystals prepared using our protocol, the statistics of avalanches follows the same pattern. In particular, similar to the case of well-annealed glasses [4, 21, 49, 62, 128, 132], the scaling behavior remains basically unchanged across the quasi-brittle yielding transition. The obtained power law range extends over up to six decades with pre-yield and post-yield energy distributions sharing the same exponent  $\epsilon = 1.0$ . The invariance of the exponent  $\epsilon$  across the yielding transition suggests that while the spatial organization of plastic events changes drastically from local and non-cooperative to global and collective, the statistical distribution of events remains insensitive to these details responding only to the global organization of the underlying energy landscape [13, 133].

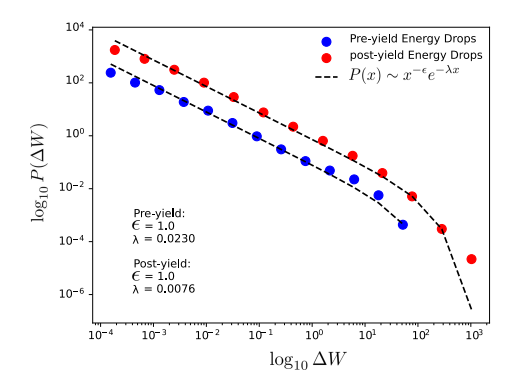


FIG. 7. Probability distribution of energy drops during avalanches in pre- and post-yield regimes.

The value of the power-law exponent  $\epsilon=1.0$  is a signature of an archetypically 'wild' crystal plasticity in the sense of [125]. The same value was obtained in discrete dislocation dynamics studies of disorder-free 2D samples containing a fixed number of preexisting dislocations [62, 134] and was also recorded in numerical experiments on pristine crystals using a scalar version of the MTM [48]. The exponent  $\epsilon=1.0$  has been previously interpreted in crystal plasticity framework as representing either dislocation jamming or self-induced glassiness [21, 135, 136].

It is rather striking that exactly the same value of the exponent has been also recorded in the studies of plastic flows in structural glasses [13, 137, 138]. A theoretical understanding of the relation between the emergence of the power law exponent  $\epsilon=1.0$  and the structure of the underlying energy landscapes has been developed in the theory of spin glasses.

Thus, it was shown that the hierarchical (ultrametric) organization of energy wells in the phase space results in an intermittent, scale-free response to quasistatic deformation [139–142]. Moreover, it was rigorously proved that in the meanfield limit the associated distribution of energy avalanches must be of a power law with exponent  $\epsilon=1.0$ . In the spin glass context it has been also understood that the reason behind this particular value of the exponent is the marginal stability of the system [139, 143, 144].

Since glasses can be viewed as liquids at a quenching threshold, their marginal stability is similar to marginality exhibited by granular matter at a jamming point. If such systems are mechanically driven, the proximity to unstable modes leads to the mixing of statics (stability) and dynamics (instability) making the mechanical response inherently intermittent [145, 146]. Similarly, since our 'quasi-amorphous crystal' emerged from arrested dynamics, one can argue that the associated self-generated disorder brought the system from a solid to an effectively glassy state. Furthermore, our results suggest that the implied marginality is not affected by the quasi-brittle yield, which apparently does not compromise the global organization of the energy landscape while, of course, affecting the reachability of its different subdomains [147–149].

Note next that the pre-yield value of the cutoff parameter  $\lambda=0.0230$  is drastically different from its post-yield value  $\lambda=0.0076$ . The approximately three-fold decrease of the value of  $\lambda$  indicates that large energy drops become substantially more probable in the post-yield regime [18, 150]. The emergent collective behavior is reflected in a much broader extent of avalanche activity which reaches the size of the system suggesting the divergence of the characteristic length  $l\sim 1/\lambda$ . The physical nature of the implied criticality is presently actively debated [48, 151–155].

Finally we mention that the observed similarity between the structure of intermittent plastic fluctuations in amorphous and crystalline solids is supported by the fact that elastoplastic models, typically used to model amorphous plasticity [24, 138, 156, 157], are very similar to the MTM which operates within basically the same finite element setting. The difference is that the phenomenological yield thresholds of elasto-plastic models are replaced in the MTM by elastic instabilities originating from the non-convexity of the energy landscape. Accordingly, the fixed linear elastic propagators are replaced by the solution 'on the fly' of the corresponding nonlinear elasticity problems. It is important that the crucial nonlinearity in the MTM is of universal geometrical nature as it originates from the exact description of finite elastic deformations.

To conclude, we showed that mechanically driven perfect crystals can exhibit quasi-brittle plastic yielding which is remarkably similar to the behavior of well-annealed glassy materials. The implied parallel features of the mechanical response emerge after pristine crystals acquire self-generated disorder resulting from massive dislocation nucleation during the breakdown of an affine elastic configuration. The ensuing quasi-amorphous crystals exhibit pre- and post-yield avalanches with power law statistics whose matching exponents are indicative of the marginality of the associated me-

chanical system. Adaptation of the same model to realistic 3D crystals will allow one to distinguish between edge and screw dislocations opening the way to the adequate account of such physically important effects as dislocation climb, cross slip and forest hardening.

Acknowledgments. The authors thank N. Gorbushin,

S. Patinet, G. Tejedor for helpful discussions. The work of O.U.S. was supported by the grants ANR-21-CE08-MESOCRYSP, ANR-20-CE91-0010, ANR-24-CE91-0002. L. T. was supported by the grants ANR-21-CE08-MESOCRYSP and ERC-H2020-MSCA-RISE-2020-101008140.

- [1] M. Zaiser, Adv. Phys. 55, 185 (2006).
- [2] W. Jian, M. Xiao, W. Sun, and W. Cai, J. Mech. Phys. Solids 186, 105577 (2024).
- [3] M. Ortiz, J. Appl. Mech. 66, 289 (1999).
- [4] S. Papanikolaou, Y. Cui, and N. Ghoniem, Modell. Simul. Mater. Sci. Eng. 26, 013001 (2017).
- [5] J. Kosterlitz, Rep. Prog. Phys. **79**, 026001 (2016).
- [6] M. Khantha and V. Vitek, Acta Mater. 45, 4675 (1997).
- [7] T. Hochrainer, S. Sandfeld, M. Zaiser, and P. Gumbsch, J. Mech. Phys. Solids 63, 167 (2014).
- [8] J. S. Langer, J. Stat. Phys. 175, 531 (2019).
- [9] P. M. Derlet and R. Maaß, J. Appl. Phys. 120, 225101 (2016).
- [10] P. D. Ispánovity, I. Groma, G. Györgyi, F. F. Csikor, and D. Weygand, Phys. Rev. Lett. 105, 085503 (2010).
- [11] K. M. Kamani and S. A. Rogers, Proc. Natl. Acad. Sci. USA 121, e2401409121 (2024).
- [12] L. Berthier, G. Biroli, M. L. Manning, and F. Zamponi, arXiv preprint arXiv:2401.09385 (2024).
- [13] B. Shang, P. Guan, and J. L. Barrat, Proc. Natl. Acad. Sci. 117, 86 (2020).
- [14] J. Shang, Y. Wang, D. Pan, Y. Jin, and J. Zhang, Proc. Natl. Acad. Sci. USA 121, e2402843121 (2024).
- [15] M. Singh, M. Ozawa, and L. Berthier, Phys. Rev. Mater. 4, 025603 (2020).
- [16] D. Richard, E. Lerner, and E. Bouchbinder, MRS Bull. 46, 902 (2021).
- [17] J. Pollard and S. M. Fielding, Phys. Rev. Res. **4**, 043037 (2022).
- [18] J. Lin, E. Lerner, A. Rosso, and M. Wyart, Proc. Natl. Acad. Sci. U. S. A. 111, 14382 (2014).
- [19] G. Parisi, I. Procaccia, C. Rainone, and M. Singh, Proc. Natl. Acad. Sci. USA 114, 5577 (2017).
- [20] P. M. Derlet and R. Maaß, Acta Mater. 209, 116771 (2021).
- [21] A. Lehtinen, G. Costantini, M. J. Alava, S. Zapperi, and L. Laurson, Phys. Rev. B 94, 064101 (2016).
- [22] J. P. Sethna, M. K. Bierbaum, K. A. Dahmen, C. P. Goodrich, J. R. Greer, L. X. Hayden, and S. Zapperi, Annu. Rev. Mater. Res. 47, 217 (2017).
- [23] M. Ovaska, A. Lehtinen, M. J. Alava, L. Laurson, and S. Zapperi, Phys. Rev. Lett. 119, 265501 (2017).
- [24] A. Nicolas, E. E. Ferrero, K. Martens, and J. Barrat, Rev. Mod. Phys. 90 (2018).
- [25] D. Rodney, A. Tanguy, and D. Vandembroucq, Model. Simul. Mat. Sci. Eng. 19, 083001 (2011).
- [26] M. Popović, T. W. J. de Geus, and M. Wyart, Phys. Rev. E 98, 040901 (2018).
- [27] A. Tanguy, C. R. Phys. 22, 117 (2021).
- [28] M. Talamali, V. Petäjä, D. Vandembroucq, and S. Roux, C. R. Mécanique 340, 275 (2012).
- [29] J. T. Parley and P. Sollich, Phys. Rev. E. 110, 045002 (2024).
- [30] S. Karmakar, E. Lerner, and I. Procaccia, Phys. Rev. E Stat. Nonlin. Soft Matter Phys. 82, 055103 (2010).
- [31] M. Ozawa, L. Berthier, G. Biroli, A. Rosso, and G. Tarjus,

- Proc. Natl. Acad. Sci. 115, 6656 (2018).
- [32] T. Divoux, E. Agoritsas, S. Aime, C. Barentin, J.-L. Barrat, R. Benzi, L. Berthier, D. Bi, G. Biroli, D. Bonn, P. Bourrianne, M. Bouzid, E. Del Gado, H. Delanoe-Ayari, K. Farain, S. Fielding, M. Fuchs, J. van der Gucht, S. Henkes, M. Jalaal, Y. M. Joshi, A. Lemaitre, R. L. Leheny, S. Manneville, K. Martens, W. C. K. Poon, M. Popovic, I. Procaccia, L. Ramos, J. A. Richards, S. Rogers, S. Rossi, M. Sbragaglia, G. Tarjus, F. Toschi, V. Trappe, J. Vermant, M. Wyart, F. Zamponi, and D. Zare, Soft Matter 20, 6868 (2024).
- [33] M. Moshe, I. Levin, H. Aharoni, R. Kupferman, and E. Sharon, Proc. Natl. Acad. Sci. 112, 10873 (2015).
- [34] M. Baggioli, M. Landry, and A. Zaccone, Phys. Rev. E. 105, 024602 (2022).
- [35] M. J. Bowick and L. Giomi, Adv. Phys. 58, 449 (2009).
- [36] M. Katanaev and I. Volovich, Annals of Physics 216, 1 (1992).
- [37] F. Sozio and A. Yavari, Math. Mech. Solids 25, 1267 (2020).
- [38] G. Picard, A. Ajdari, F. Lequeux, and L. Bocquet, Europhysics Journal E 15, 371 (2004).
- [39] Z. Budrikis, D. Castellanos, S. Sandfeld, M. Zaiser, and S. Zapperi, Nat. Commun. **8**, 15928 (2017).
- [40] W. Cai, A. Arsenlis, C. R. Weinberger, and V. V. Bulatov, J. Mech. Phys. Solids 54, 561 (2006).
- [41] O. U. Salman and L. Truskinovsky, Phys. Rev. Lett. 106, 175503 (2011).
- [42] O. U. Salman and L. Truskinovsky, Int. J. Eng. Sci. 59, 219 (2012).
- [43] R. Baggio, E. Arbib, P. Biscari, S. Conti, L. Truskinovsky, G. Zanzotto, and O. U. Salman, Phys. Rev. Lett. 123, 205501 (2019).
- [44] O. U. Salman, R. Baggio, B. Bacroix, G. Zanzotto, N. Gorbushin, and L. Truskinovsky, C. R. Phys. 22, 201 (2021).
- [45] N. Perchikov and L. Truskinovsky, J. Mech. Phys. Solids 190, 105704 (2024).
- [46] R. Baggio, O. U. Salman, and L. Truskinovsky, Eur. J. Mech. A/Solids 99, 104897 (2023).
- [47] R. Baggio, O. U. Salman, and L. Truskinovsky, Phys. Rev. E 107, 025004 (2023).
- [48] P. Zhang, O. U. Salman, J. Weiss, and L. Truskinovsky, Phys. Rev. E 102, 023006 (2020).
- [49] J. Weiss, P. Zhang, O. U. Salman, G. Liu, and L. Truskinovsky, C. R. Phys. 22, 163 (2021).
- [50] A. Arsenlis, W. Cai, M. Tang, M. Rhee, T. Oppelstrup, G. Hommes, T. G. Pierce, and V. V. Bulatov, Modell. Simul. Mater. Sci. Eng. 15, 553 (2007).
- [51] L. A. Zepeda-Ruiz, A. Stukowski, T. Oppelstrup, N. Bertin, N. R. Barton, R. Freitas, and V. V. Bulatov, Nat. Mater. 20, 315 (2021).
- [52] M. Ponga, K. Bhattacharya, and M. Ortiz, J. Comput. Phys. 407, 109249 (2020).
- [53] P. Lafourcade, G. Ewald, T. Carrard, and C. Denoual, Mech. Mater. 200, 105189 (2025).
- [54] P. Chan, G. Tsekenis, J. Dantzig, K. A. Dahmen, and N. Gold-

- enfeld, Phys. Rev. Lett. 105, 015502 (2010).
- [55] M. Salvalaglio, L. Angheluta, Z. Huang, A. Voigt, K. R. Elder, and J. Viñals, J. Mech. Phys. Solids 137, 103856 (2020).
- [56] Z. Zhong, Y. Huang, Y. Gao, R. Li, S. Yao, K. Wang, W. Zhu, and W. Hu, Physica B Condens. Matter 706, 417154 (2025).
- [57] M. Javanbakht and V. I. Levitas, Int. J. Solids Struct. 82, 95 (2016).
- [58] I. J. Beyerlein and A. Hunter, Philos. Trans. A Math. Phys. Eng. Sci. 374 (2016).
- [59] M. Koslowski, A. M. Cuitiño, and M. Ortiz, J. Mech. Phys. Solids 50, 2597 (2002).
- [60] Y. U. Wang, Y. M. Jin, and A. G. Khachaturyan, Acta Mater. 51, 4209 (2003).
- [61] B. Devincre, T. Hoc, and L. Kubin, Science 320, 1745 (2008).
- [62] P. D. Ispánovity, L. Laurson, M. Zaiser, I. Groma, S. Zapperi, and M. J. Alava, Phys. Rev. Lett. 112, 235501 (2014).
- [63] D. Gómez-García, B. Devincre, and L. P. Kubin, Phys. Rev. Lett. 96, 125503 (2006).
- [64] G. Po, M. Lazar, D. Seif, and N. Ghoniem, J. Mech. Phys. Solids (2014).
- [65] S. Lu, J. Zhao, M. Huang, Z. Li, G. Kang, and X. Zhang, Int. J. Plast. 156, 103356 (2022).
- [66] N. Bertin, V. V. Bulatov, and F. Zhou, Npj Comput. Mater. 10, 1 (2024).
- [67] T. Nasir Tak and P. J. Guruprasad, Model. Simul. Mat. Sci. Eng. 33, 045001 (2025).
- [68] K. Starkey, G. Winther, and A. El-Azab, J. Mech. Phys. Solids 139, 103926 (2020).
- [69] Y. Zhang, R. Wu, and M. Zaiser, Model. Simul. Mat. Sci. Eng. 33 (2025).
- [70] A. Acharya, J. Mech. Phys. Solids 161 (2022).
- [71] A. Acharya, A. R., and A. Sawant, Scr. Mater. 54, 705 (2006).
- [72] D. Rodney and R. Phillips, Phys. Rev. Lett. 82, 1704 (1999).
- [73] B. Van Koten and B. Luskin, SIAM J. Numer. Anal. 49, 2182 (2011).
- [74] R. Miller and E. Tadmor, J. Comput.-Aided Mater. Des. 9, 203 (2002).
- [75] Z. Zhang, J. Zhang, Y. Ni, C. Wang, K. Jiang, and X. Ren, in *The 1st International Electronic Conference on Crystals*, Vol. 7 (MDPI, 2018) p. 1113.
- [76] P. Engel, Geometric Crystallography: An Axiomatic Introduction to Crystallography (Springer Netherlands, 1986).
- [77] L. Michel, Phys. Rep. 341, 265 (2001).
- [78] R. L. E. Schwarzenberger, Proc. Cambridge Phil. Soc. 72, 325 (1972).
- [79] M. Pitteri and G. Zanzotto, Continuum models for phase transitions and twinning in crystals (Chapman and Hall/CRC, Boca Raton, 2002).
- [80] J. L. Ericksen, Int. J. Solids Struct. 6, 951 (1970).
- [81] J. L. Ericksen, in *Nonlinear Elasticity*, edited by R. W. Dickey (Academic Press, New York, 1973) pp. 161–173.
- [82] J. L. Ericksen, Adv. Appl. Mech. 17, 189 (1977).
- [83] J. L. Ericksen, Arch. Ration. Mech. Anal. 73, 99 (1980).
- [84] J. L. Ericksen, Arch. Ration. Mech. Anal. 107, 23 (1989).
- [85] G. Parry, Math. Proc. Cambridge Philos. Soc. **80**, 189 (1976).
- [86] G. P. Parry, in *Mathematical Proceedings of the Cambridge Philosophical Society*, Vol. 82 (Cambridge University Press, 1977) pp. 165–175.
- [87] G. P. Parry, Arch. Rational Mech. Anal. 145, 1 (1998).
- [88] I. Folkins, J. Math. Phys. 32, 1965 (1991).
- [89] S. Conti and G. Zanzotto, Arch. Ration. Mech. Anal. 173, 69 (2004).
- [90] K. Bhattacharya, S. Conti, G. Zanzotto, and J. Zimmer, Nature 428, 55 (2004).

- [91] C. Denoual, A. Caucci, L. Soulard, and Y. Pellegrini, Phys. Rev. Lett. 105, 035703 (2010).
- [92] Y. Gao, Y. Wang, and Y. Zhang, IUCrJ 6, 96 (2019).
- [93] Y. Gao, Y. Zhang, and Y. Wang, Acta Mater. 196, 280 (2020).
- [94] Y. Gao, Materialia 9, 100588 (2020).
- [95] Y. Gao, T. Yu, and Y. Wang, Shap. Mem. Superelasticity 6, 115 (2020).
- [96] Y. Gao, Y. Zhang, L. K. Aagesen, J. Yu, M. Long, and Y. Wang, Phys. Rev. Res. 2, 013146 (2020).
- [97] P. Biscari, M. Urbano, A. Zanzottera, and G. Zanzotto, J. Elast. 123, 85 (2015).
- [98] E. Arbib, P. Biscari, L. Bortoloni, C. Patriarca, and G. Zanzotto, Int. J. Plast. 130, 102728 (2020).
- [99] E. Arbib, P. Biscari, C. Patriarca, and G. Zanzotto, J. Elast. 155, 747 (2023).
- [100] E. Arbib, N. Barrera, P. Biscari, and G. Zanzotto, J. Appl. Mech. 92, 1 (2025).
- [101] "Supplemental material," See Supplemental Material at url for details on the fundamental domains, the specific elastic energy density function, the numerical method, and the implementation of the loading conditions.
- [102] G. Puglisi and L. Truskinovsky, J. Mech. Phys. Solids 53, 655 (2005).
- [103] H. C. Simpson and S. J. Spector, in Mechanics and Thermodynamics of Continua: A Collection of Papers Dedicated to BD Coleman on His Sixtieth Birthday (Springer Berlin Heidelberg, Berlin, Heidelberg, 1989) pp. 159–179.
- [104] Y. Grabovsky and L. Truskinovsky, J. Nonlinear Sci. 23, 891
- [105] D. J. Steigmann, M. Bîrsan, and M. Shirani, in Lecture Notes on the Theory of Plates and Shells: Classical and Modern Developments (Springer Nature Switzerland, Cham, 2023) pp. 61–76.
- [106] R. Maaß and P. M. Derlet, Acta Mater. 143, 338 (2018).
- [107] G. Sparks and R. Maaß, Phys. Rev. Mater. 2, 120601 (2018).
- [108] G. Sparks, Y. Cui, G. Po, Q. Rizzardi, J. Marian, and R. Maaß, Phys. Rev. Mater. 3, 080601 (2019).
- [109] Q. Rizzardi, P. M. Derlet, and R. Maaß, Phys. Rev. Mater. 6, 073602 (2022).
- [110] J. Duan, Y. J. Wang, L. H. Dai, and M. Q. Jiang, Phys. Rev. Mater. 7 (2023).
- [111] H. Bei, S. Shim, G. M. Pharr, and E. P. George, Acta Mater. 56, 4762 (2008).
- [112] D. Chrobak, N. Tymiak, A. Beaber, O. Ugurlu, W. W. Gerberich, and R. Nowak, Nat. Nanotechnol. 6, 480 (2011).
- [113] Z. Wang, Z. Shan, J. Li, J. Sun, and E. Ma, Acta Mater. 60, 1368 (2012).
- [114] Y. Cui, G. Po, and N. Ghoniem, Phys. Rev. B 95, 064103 (2017).
- [115] J. R. Greer and J. T. M. D. Hosson, Prog. Mater Sci. **56**, 654 (2011).
- [116] S. S. Brenner, J. Appl. Phys. 27, 1484 (1956).
- [117] S. S. Brenner, Science 128, 569 (1958).
- [118] A. Sharma, J. Hickman, N. Gazit, E. Rabkin, and Y. Mishin, Nat. Commun. 9, 4102 (2018).
- [119] D. Mordehai, O. David, and R. Kositski, Adv. Mater. 30, e1706710 (2018).
- [120] E. T. Lilleodden and W. D. Nix, Acta Mater. 54, 1583 (2006).
- [121] S. G. Corcoran, R. J. Colton, E. T. Lilleodden, and W. W. Gerberich, Phys. Rev. B Condens. Matter 55, R16057 (1997).
- [122] A. P. Sutton, Int. Met. Rev. 29, 377 (1984).
- [123] L. Priester, *Grain boundaries: from theory to engineering* (Springer Science & Business Media, 2012).
- [124] V. Randle, The role of the coincidence site lattice in grain

- boundary engineering (CRC Press, London, England, 2024).
- [125] J. Weiss, W. B. Rhouma, T. Richeton, S. Dechanel, F. Louchet, and L. Truskinovsky, Phys. Rev. Lett. 114, 105504 (2015).
- [126] J. M. Tarp, L. Angheluta, J. Mathiesen, and N. Goldenfeld, Phys. Rev. Lett. 113, 265503 (2014).
- [127] M. C. Miguel and S. Zapperi, Science 312, 1151 (2006).
- [128] M. J. Alava, L. Laurson, and S. Zapperi, Eur. Phys. J. Spec. Top. 223, 2353 (2014).
- [129] B. Tyukodi, C. A. Lemarchand, J. S. Hansen, and D. Vandembroucq, Phys. Rev. E. 93, 023004 (2016).
- [130] E. Lerner, I. Procaccia, C. Rainone, and M. Singh, Phys. Rev. E 98, 063001 (2018).
- [131] M. Ozawa, L. Berthier, G. Biroli, and G. Tarjus, Phys. Rev. Res. 4 (2022).
- [132] J. P. Sethna, K. A. Dahmen, and C. R. Myers, Nature **410**, 242 (2001)
- [133] N. Oyama, H. Mizuno, and A. Ikeda, Phys. Rev. E. 104, 015002 (2021).
- [134] H. Salmenjoki, L. Laurson, and M. J. Alava, Phys. Rev. Mater. 5, 073601 (2021).
- [135] M. Ovaska, L. Laurson, and M. J. Alava, Sci. Rep. 5, 10580 (2015).
- [136] X. Zhang, X. Zhang, Q. Li, and F. Shang, Chin. Physics Lett. 33, 106401 (2016).
- [137] B. Tyukodi, D. Vandembroucq, and C. E. Maloney, Phys. Rev. E **100**, 043003 (2019).
- [138] E. E. Ferrero and E. A. Jagla, Soft Matter 15, 9041 (2019).
- [139] S. Franz and S. Spigler, Phys. Rev. E 95, 022139 (2017).
- [140] M. Müller and M. Wyart, Annu. Rev. Condens. Matter Phys. 6, 177 (2015).
- [141] L. Berthier, G. Biroli, P. Charbonneau, E. I. Corwin, S. Franz, and F. Zamponi, J. Chem. Phys. 151, 010901 (2019).
- [142] R. C. Dennis and E. I. Corwin, Phys. Rev. Lett. 124, 078002

- (2020).
- [143] F. Pázmándi, G. Zaránd, and G. T. Zimányi, Phys. Rev. Lett. 83, 1034 (1999).
- [144] P. Doussal, M. Müller, and K. J. Wiese, Phys. Rev. B Condens. Matter Mater. Phys. 85 (2012).
- [145] K. Lamp, N. Küchler, and J. Horbach, J. Chem. Phys. 157 (2022).
- [146] S. Rossi and G. Tarjus, J. Stat. Mech. 2022, 093301 (2022).
- [147] I. Regev and T. Lookman, in *Understanding Complex Systems*, Understanding complex systems (Springer International Publishing, Cham, 2017) pp. 227–259.
- [148] I. Regev and T. Lookman, J. Phys. Condens. Matter 31 (2017).
- [149] I. Regev, I. Attia, K. Dahmen, S. Sastry, and M. M., Phys. Rev. E. 103, 062614 (2021).
- [150] C. Ruscher and J. Rottler, Tribol. Lett. **69**, 64 (2021).
- [151] G. Grinstein, in Scale Invariance, Interfaces, and Non-Equilibrium Dynamics (Springer US, Boston, MA, 1995) pp. 261–293.
- [152] A. Zippelius, M. Fuchs, A. Rosso, J. P. Sethna, and M. Wyart, in *Spin Glass Theory and Far Beyond* (WORLD SCIEN-TIFIC, 2023) pp. 277–305.
- [153] P. Charbonneau, E. Marinari, G. Parisi, F. Ricci-tersenghi, G. Sicuro, F. Zamponi, and M. M. (Eds.)., Spin glass theory and far beyond: replica symmetry breaking after 40 years (World Scientific, 2023).
- [154] N. Oyama, H. Mizuno, and A. Ikeda, Soft Matter 19, 6074 (2023).
- [155] Y. Xing, Y. Yuan, H. Yuan, S. Zhang, Z. Zeng, X. Zheng, C. Xia, and Y. Wang, Nat. Phys. 20, 646 (2024).
- [156] S. Rossi, G. Biroli, M. Ozawa, G. Tarjus, and F. Zamponi, Phys. Rev. Lett. 129, 228002 (2022).
- [157] D. Fernández Castellanos, S. Roux, and S. Patinet, C. R. Phys. 22, 135 (2021).

## **Quasi-amorphous crystals: Supplemental Material**

O.U. Salman,<sup>1,2</sup> A. Ahadi,<sup>2</sup> and L. Truskinovsky<sup>3</sup>

<sup>1</sup>LSPM, CNRS UPR3407, Université Sorbonne Paris Nord, 93400, Villateneuse, France <sup>2</sup>Lund University, Department of Mechanical Engineering Sciences, SE-221 00 Lund, Sweden <sup>3</sup>PMMH, CNRS UMR 7636 ESPCI PSL, 10 Rue Vauquelin, 75005, Paris, France (Dated: November 12, 2025)

a. Fundamental and elastic domains. Consider the energy density function  $\varphi(\mathbf{C})$  with tensorial symmetry  $GL(2,\mathbb{Z})=\{\mathbf{m},\,m_{IJ}\in\mathbb{Z},\,\det(\mathbf{m})=\pm 1\}$ . We refer to the restriction of such periodic energy density to the minimal periodicity (fundamental) domain as  $\varphi_{\mathscr{D}}(\tilde{\mathbf{C}})$ . Here  $\tilde{\mathbf{C}}=\mathbf{m}^T\mathbf{C}\mathbf{m}$  is the projection of a general metric tensor  $\mathbf{C}$  into the domain  $\mathscr{D}$  and  $\mathbf{m}$  is the corresponding unimodular integer valued matrix that performs the projection while ensuring that  $\varphi(\mathbf{C})=\varphi_{\mathscr{D}}(\tilde{\mathbf{C}})$ . The actual configuration of the fundamental domain  $\mathscr{D}$  is well known [1–4]

$$\mathscr{D} = \left\{ 0 < C_{11} \le C_{22}, \quad 0 \le C_{12} \le \frac{C_{11}}{2} \right\}, \tag{1}$$

where  $\det \mathbf{C}=1$ . Given a generic metric  $\mathbf{C}$ , the task of finding a unimodular matrix  $\mathbf{m}$  ensuring that  $\tilde{\mathbf{C}}\in \mathscr{D}$  (and therefore  $\varphi(\mathbf{C})=\varphi_{\mathscr{D}}(\tilde{\mathbf{C}})$ ) can be formulated as a recursive algorithm which is also well known (Lagrange reduction) [2, 3]. Specifically, if we define the matrices

$$\mathbf{m}_1 = \begin{pmatrix} 1 & 0 \\ 0 & -1 \end{pmatrix}, \ \mathbf{m}_2 = \begin{pmatrix} 0 & 1 \\ 1 & 0 \end{pmatrix}, \ \mathbf{m}_3 = \begin{pmatrix} 1 & -1 \\ 0 & 1 \end{pmatrix}, \ (2)$$

and start with an assumption that m = I, we can proceed through the following steps: (i ) if  $C_{12} < 0$ , change sign of  $C_{12}$  using the mapping  $\mathbf{m} \to \mathbf{mm}_1$ ; (ii) if  $C_{22} < C_{11}$ , swap these two components using the mapping  $\mathbf{m} \rightarrow \mathbf{m}\mathbf{m}_2$ ; (iii) if  $2C_{12} > C_{11}$ , set  $C_{12} = C_{12} - C_{11}$  using the mapping  $\mathbf{m} \to \mathbf{mm}_3$ . Note that the action of  $\mathbf{m}_1$  is a reflection that ensures an acute angle between two lattice vectors of the square lattice  $e_i$  where i = 1, 2; the action of the matrix  $m_2$  is also a reflection as it swaps two lattice vectors  $e_i$ . Both of these operations belong to the point group and propagate the metric only inside the corresponding 'elastic domain' (Ericksen-Pitteri neighborhood) composed of the four copies of the minimal domain  $\mathcal{D}$  [4, 5]. Instead, the mapping defined by matrix m<sub>3</sub> brings the metric outside the 'elastic domain' and therefore represents a quantized analog of the macroscopic plastic strain.

b. Elastic energy density. While the single-period Landau potential  $\varphi_{\mathscr{D}}(\mathbf{C})$  can be constructed using the classical Cauchy-Born approach, see for instance [5, 6], in this paper we used, for simplicity, the phenomenological expression proposed in [2]. Specifically, the elastic energy density is represented as a sum of two terms:

$$\varphi(\tilde{\mathbf{C}}) = \varphi_0 \left( \frac{\tilde{\mathbf{C}}}{(\det \tilde{\mathbf{C}})^{1/2}} \right) + \varphi_v(\det \tilde{\mathbf{C}}),$$
(3)

where  $\varphi_0$  accounts for contributions due to shear while  $\varphi_v$  penalizes volumetric deformations. The  $GL(2,\mathbb{Z})$  invariant

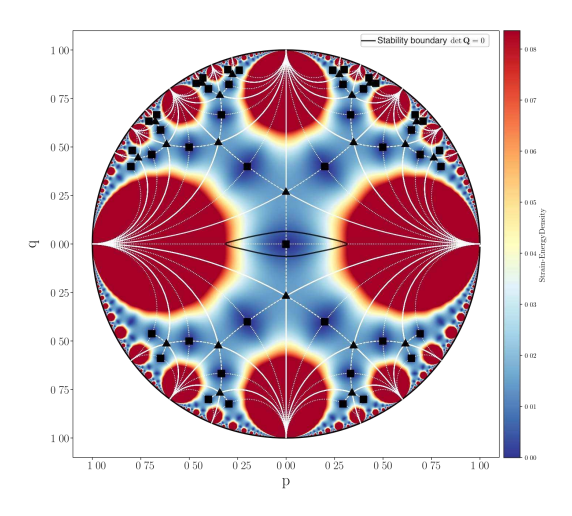


FIG. 1. Strain-energy density in the configurational space  $C_{11}, C_{22}, C_{12}$  with  $\det \mathbf{C} = 1$  stereographically projected on the Poincaré disk. Thin white lines represent the  $GL(2,\mathbb{Z})$  tessellation of the a Poincaré disk into equivalent periodicity domains. Colors represent energy levels. Elastic stability boundary given by (10) is shown by the thick black contour surrounding the reference state. Small black squares and triangles correspond to equivalent square and triangular lattices, respectively.

shear term is chosen in the form a sixth-order polynomial which is the minimal requirement ensuring stress continuity over the whole configurational space [1, 2]. It depends on a single parameter  $\beta$  allowing one to associate ground state either with square or triangular (hexagonal) lattice

$$\varphi_0\left(\frac{\tilde{\mathbf{C}}}{(\det \tilde{\mathbf{C}})^{1/2}}\right) = \beta \psi_1\left(\frac{\tilde{\mathbf{C}}}{(\det \tilde{\mathbf{C}})^{1/2}}\right) + \psi_2\left(\frac{\tilde{\mathbf{C}}}{(\det \tilde{\mathbf{C}})^{1/2}}\right). \tag{4}$$

The requirement of stress continuity across the whole periodic energy landscape specifies the functions  $\psi_1$  and  $\psi_2$ 

$$\psi_1 = I_1^4 I_2 - \frac{41}{99} I_2^3 + \frac{7}{66} I_1 I_2 I_3 + \frac{1}{1056} I_3^2, \tag{5}$$

$$\psi_2 = \frac{4}{11}I_2^3 + I_1^3I_3 - \frac{8}{11}I_1I_2I_3 + \frac{17}{528}I_3^2.$$
 (6)

where we used the known hexagonal invariants of the metric tensor

$$I_{1} = \frac{1}{3} (\tilde{C}_{11} + \tilde{C}_{22} - \tilde{C}_{12}), \tag{7}$$

$$I_{2} = \frac{1}{4} (\tilde{C}_{11} - \tilde{C}_{22})^{2} + \frac{1}{12} (\tilde{C}_{11} + \tilde{C}_{22} - 4\tilde{C}_{12})^{2}, \tag{8}$$

$$I_{3} = (\tilde{C}_{11} - \tilde{C}_{22})^{2} (\tilde{C}_{11} + \tilde{C}_{22} - 4\tilde{C}_{12}) - \frac{1}{9} (\tilde{C}_{11} + \tilde{C}_{22} - 4\tilde{C}_{12})^{3}.$$

$$(9)$$

We select  $\beta = -1/4$  to ensure that global energy minimizers correspond to square lattices. The volumetric part of the energy density, which primarily influences the fine structure of the dislocation cores and also controls the formation of voids, is assumed to be of a generic form preventing infinite compression  $\varphi_v(s) = \mu(s - \log(s))$ . To keep in our numerical experiments the strain field close to the surface  $\det \mathbf{C} = 1$ , we adopted a sufficiently high value of the bulk modulus,  $\mu = 5$ .

The isochoric part of the energy landscape is illustrated in Fig. 2 of the main paper. Here we also show the same Landautype potential in Fig. 1, but now in the level set representation. Dark blue regions correspond to the equivalent square energy wells. Red domains show effectively inaccessible regions where the energy is very high (truncated). Relatively low energy valleys colored in yellow correspond roughly to two simple shear plastic 'mechanisms' available in square lattices.

c. Internal length scale. The lack of convexity of the potential is a property which the MTM shares with other similar Landau-type continuum theories. In the MTM approach the necessary regularization is introduced by bringing into the model an internal scale h through explicit spatial discretization. If L is the linear size of the macroscopic domain and  $N^2$ is the number of nodes in the mesoscopic grid, then the parameter h = L/N introduces elastic finite elements imitating mesoscopic aggregates of atomic particles and defines in this way the cutoff beyond which the deformation is considered homogeneous (affine). The corresponding small parameter is  $\delta = h/L = 1/N$ . Another small parameter in the problem is  $\epsilon = a/L$  where a is the interatomic distance and we are interested in the double limit:  $\epsilon \to 0$  and  $\delta \to 0$  while  $\delta \gg \epsilon$ . In the MTM approach we first implicitly perform the limit  $\epsilon \to 0$  and recover in this way the continuum constitutive response using the Cauchy-Born rule. Then instead of performing the classical  $\delta \to 0$  and obtaining the conventional scale-free continuum theory, we preserve in the theory a small but finite value of the parameter  $\delta$ . In this way we effectively account for finite size effects. In particular, the size of the dislocation cores is overestimated while the number of dislocations is underestimated. However, the resulting approach preserves the basic nature of both long-range and short-range interactions of dislocations at least when they are away from the boundaries. For instance, the blown up dislocations will still nucleate and self-lock adequately.

In our numerical code we used dimensionless parameters  $\tilde{h}=h/b=1$  and  $\tilde{L}=L/b=1/N$ , where the b is the

size of the mesoscopic particle. For the choice of the scale b it is natural to require that the Cauchy-Born energy density computed for a lattice fragment with scale b exhibits a high level of periodicity within the range of strains reached in a particular numerical experiment. We have checked that in our case the assumption that  $b\sim 10a$  is sufficient.

d. Numerical method. Numerical implementation of the MTM approach reduces to solving an elastic finite element problem. The goal is to follow the displacements of the network of discrete nodes labeled by integer-valued coordinates  $I=1,...,N^2$ .

Specifically, we assume that each of the elements is a deformable triangle and employ the standard linear 3-node elements [7, 8]. The displacement field inside each of the elements, represented in dimensionless form, can be written in the form  $\mathbf{u}(\mathbf{z}) = \sum_a \mathcal{N}^a(\mathbf{z};h)\mathbf{u}^a$ , where  $\mathcal{N}^a(\mathbf{z};\mathbf{h})$  are compactly supported linear shape functions,  $\mathbf{u}^a$  are the are the nodal displacements and summation is assumed over repeated indexes; the interpolation functions for each element are defined in terms of a local dimensionless coordinate system. The mesoscopic deformation gradient is then  $\mathbf{F}(\mathbf{z};h) = \mathbb{I} + \mathbf{u}^a \otimes \nabla \mathcal{N}^a(\mathbf{z};h)$ .

In terms of macroscopic reference coordinates, the elastic energy inside each element can be computed using the simplest quadrature scheme  $w(\mathbf{x};h) = \frac{1}{2}\varphi(\mathbf{F}(\mathbf{x};h))J(\mathbf{x},h)$ , where J is the Jacobian of the transformation from local (z) to global (x) coordinate system. Note that in view of our assumptions the energy of a deformed triangular element depends on three parameters: the deformed lengths of the bonds and the deformed value of the angle between them.

Finding a solution of an elastic problem implies local minimization of the energy  $W=\int_{\Omega}w(\mathbf{x};h)d\mathbf{x}$ , which is prescribed on a triangulated domain  $\Omega$ . The conditions of mechanical equilibrium take the form  $\nabla\cdot\mathbf{P}=0$  where we introduced the first Piola-Kirchhoff stress tensor

$$\mathbf{P} = 2\mathbf{Fm}\mathbf{\Sigma}\mathbf{m}^T,$$

with

$$\boldsymbol{\Sigma} = \begin{bmatrix} \frac{\partial w}{\partial \tilde{C}11} & \frac{1}{2} \frac{\partial w}{\partial \tilde{C}12} \\ \frac{1}{2} \frac{\partial w}{\partial \tilde{C}12} & \frac{\partial w}{\partial \tilde{C}22} \end{bmatrix}.$$

In the finite element representation these equations reduce to

$$\frac{\partial W}{\partial \mathbf{u}^a} = \int_{\Omega} \mathbf{P}(\mathbf{x}; h) \nabla \mathcal{N}^a(\mathbf{x}; h) d\mathbf{x} = 0.$$

The ensuing nonlinear equilibrium problem is solved numerically using the L-BFGS algorithm [9], which constructs a positive definite approximation to the Hessian, enabling quasi-Newton steps that progressively reduce the total energy. Iterations continue until the energy change per iteration falls below a prescribed tolerance. At each iteration, starting from an approximate solution  $\mathbf{w}^a$ , we compute a displacement correction  $d\mathbf{w}^a = \mathbf{u}^a - \mathbf{w}^a$  by solving the linearized equilibrium equations via LU factorization [10, 11]:

$$K_{ij}^{ab}dw_j^b + R_i^a = 0,$$

where

$$K_{ij}^{ab} = A_{ipjq}(\mathbf{F}) \frac{\partial \mathcal{N}^a}{\partial x_p} \frac{\partial \mathcal{N}^b}{\partial x_q}$$

is the global stiffness matrix and

$$R_i^a = P_{ip}(\mathbf{F}) \frac{\partial \mathcal{N}^a}{\partial x_p},$$

is the residual force vector with summation implied over repeated indices. Note that we introduced the tensor of tangential elastic moduli

$$A_{iajb} = \frac{\partial^2 \varphi_{\mathscr{D}}(\tilde{\mathbf{C}})}{\partial F_{ia} \partial F_{jb}}.$$

which can be used construct the Eulerian acoustic tensor

$$Q_{ij} = F_{la}F_{mb}A_{iajb}n_ln_m,$$

where n is an arbitrary unit vector. The Legendre-Hadamard condition which marks the threshold of elastic instability in continuum theory can be then written in the form

$$\det(\mathbf{Q}) = 0. \tag{10}$$

The corresponding stability boundary is referred to in the main paper and it is illustrated for the chosen elastic energy landscape in Fig. 1.

e. Implementation of the loading conditions. To simulate an effectively infinite crystal under controlled macroscopic affine deformation, we use the method of domain replication. Starting from the computational domain  $\Omega_0$  with dimensions  $L_x \times L_y$ , we generate a periodic lattice of domains using translation vectors  $\mathbf{t}_n = \begin{pmatrix} n_x L_x \\ n_y L_y \end{pmatrix}$ , where  $\mathbf{n} = (n_x, n_y) \in \{-1, 0, 1\}^2$ . Let  $\bar{\mathbf{F}}(\alpha)$  denote the macroscopic deformation gradient tensor at the parameter value  $\alpha$ . Under such affine deformation, the position of replicated domains relative to the central domain  $\Omega_0$  is given by:  $\mathbf{R}_n = \bar{\mathbf{F}}(\alpha) \cdot \mathbf{t}_n$ , where  $\mathbf{R}_n$  represents the displacement vector of the origin of the domain associated with  $\mathbf{t}_n$ . Then, for a node located at position  $\mathbf{x}_i$  in the central domain  $\Omega_0$ , its periodic affine and the sum of th

riodic image, associated with the translation vector  $\mathbf{t}_n$ , is at:

 $\mathbf{x}_i^{(n)} = \mathbf{x}_i + \mathbf{R}_n = \mathbf{x}_i + \bar{\mathbf{F}}(\alpha) \cdot \mathbf{t}_n$ . Such correspondence

ensures that the macroscopic deformation gradient  $\bar{\mathbf{F}}(\alpha)$  is

consistently applied across all periodic images of  $\Omega_0$ . After

establishing the positions of all nodes across the nine domains

[1] G. P. Parry, Arch. Rational Mech. Anal. **145**, 1 (1998).

(original domain  $\Omega_0$  and its eight periodic images), we perform a Delaunay triangulation on the complete set of particles:  $\mathcal{P} = \{\mathbf{x}_i : i \in \mathcal{I}_0\} \cup \{\mathbf{x}_i^{(n)} : i \in \mathcal{I}_0, n \neq \mathbf{0}\}$ , where  $\mathcal{I}_0$  denotes the set of particle indices in the original domain and  $\mathbf{0} = (0,0)$  corresponds to the null translation vector. Using the obtained global triangulation  $\mathcal{T}$ , we select the triangles that have at least one vertex belonging to the original domain  $\Omega_0$ .

Note that since triangles near periodic boundaries may be counted multiple times through different domain images, we need to ensure uniqueness by mapping all vertex indices to

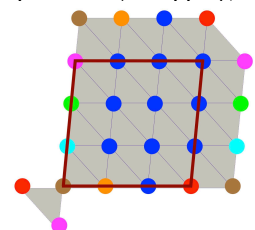


FIG. 2. The periodicity unit of the computational mesh  $\mathcal{T}_{ch}$  obtained by periodic Delaunay triangulation. The central computational domain  $\Omega_0$  is limited by the brown box. Only triangles with at least one vertex in  $\Omega_0$  are selected for the mesh (shown by the thin lines), ensuring proper connectivity across periodic boundaries while avoiding redundant counting of triangles.

their representatives in  $\Omega_0$  and using the sorted tuple of these representatives as a canonical identifier.

Specifically, a triangle is included in the chosen mesh  $\mathcal{T}_{ch}$  only upon its first encounter, ensuring that each physical triangle is counted exactly once. The ensuing periodicity unit of the computational mesh  $\mathcal{T}_{ch}$  is illustrated in Fig. 2, where we show the central domain  $\Omega_0$  (limited by the brown box) together with triangles associated with the nodes constituting this domain. Such selection procedure ensures that: (i) Each triangle in the computational mesh is counted exactly once, eliminating redundancy from the periodic extension; (ii) All triangles connected to the original domain are included, maintaining proper connectivity across periodic boundaries; (iii) The triangulation naturally incorporates the macroscopic deformation through the deformed positions of the periodic images.

The selected set of triangles  $\mathcal{T}_{ch}$  was used as the computational mesh in the MTM based numerical experiments ensuring both, compatibility with the periodic boundary conditions and consistency with the applied macroscopic deformation gradient  $\bar{\mathbf{F}}(\alpha)$ .

<sup>[2]</sup> S. Conti and G. Zanzotto, Arch. Ration. Mech. Anal. 173, 69 (2004).

<sup>[3]</sup> P. Engel, Geometric Crystallography: An Axiomatic Introduction To Crystallography (Springer Science & Business Media, Dordrecht, 2012).

<sup>[4]</sup> M. Pitteri and G. Zanzotto, Continuum models for phase tran-

sitions and twinning in crystals (Chapman and Hall/CRC, Boca Raton, 2002).

<sup>[5]</sup> R. Baggio, O. U. Salman, and L. Truskinovsky, Eur. J. Mech. A/Solids 99, 104897 (2023).

<sup>[6]</sup> R. Baggio, O. U. Salman, and L. Truskinovsky, Phys. Rev. E 107, 025004 (2023).

<sup>[7]</sup> B. M. Irons, AIAA J. 4, 2035 (1966).

- [8] J. H. Bramble and M. Zlámal, Math. Comp. 24, 809 (1970).
- [9] S. Bochkanov and V. Bystritsky, Available from: www alglib net (2013).
- [10] C. Sanderson and R. Curtin, J Open Source Softw 1, 26 (2016).
- [11] M. Fishman, S. White, and E. Stoudenmire, SciPost Phys. Codebases , 004 (2022).